https://doi.org/10.5194/egusphere-2025-5890
Preprint. Discussion started: 6 January 2026

Quantifying and Attributing CO Emissions over Central Asia using TROPOMI and Explicit Observational Uncertainty

Ye Feng[1], Jason Blake Cohen [1,*], Xiaolu Li[2], Lingxiao Lu[1], Zhewen Liu[1], Lei Wang[1], Jian Liu[3], Kai Qin[1]

[1] School of Environment and Spatial Informatics, China University of Mining Technology, Xuzhou, 221008, China
[2] School of Geographic Sciences, Taiyuan Normal University, Jinzhong, 030619, China
[3] College of Environment and Ecology, Taiyuan University of Technology, Taiyuan, 030024, China

Correspondence to: Jason Blake Cohen (jasonbc@alum.mit.edu)

Abstract: Carbon monoxide (CO) is a crucial atmospheric constituent influencing both air quality and climate. Using TROPOMI CO and HCHO column retrievals within the Model-Free Inversion Estimation Framework (MFIEF), this study quantified daily, gridded CO emissions in Central Asia (Xinjiang-China, Kazakhstan, Kyrgyzstan, and Uzbekistan) for 2019–2024. Results reveal a marked interannual decline of ~38% in mean emissions, accompanied by a weakening of emission hotspots. Seasonal peaks in winter and early spring highlight the roles of heating and industrial demand. Importantly, explicit perturbation-based uncertainty analysis showed that ~69% of grid-level estimates are unreliable if observational uncertainties are ignored or using an overly simplified emissions estimation approach, underscoring the nonlinear propagation of retrieval errors. By integrating coal consumption data, we confirm the consistency between satellite-inferred emissions and bottom-up activity estimates, while also identifying missing sources such as underground coal fires. This study demonstrates the effectiveness of MFIEF in data-scarce regions, provides actionable insights for inventory improvement and mitigation strategies, and highlights the framework's potential extension to CH_4 and CO_2 retrieval-based emission estimation.

Keywords: CO emissions; TROPOMI; Spatiotemporal distribution; Uncertainty analysis; Central Asia

1. Introduction

Air pollution and climate change are significant environmental problems resulting from economic development, urbanization, energy consumption, and transportation (Adams et al., 2020; Bel and Holst, 2018; Liang et al., 2019). CO is one of the lesser considered short-lived climate pollutants (Hanaoka and Masui, 2020; Khalil and Rasmussen, 1988, 1984; Szopa et al., 2021). It is a major sink of the hydroxyl radical (OH) affecting the concentrations of methane (CH_4) and ozone (O_3) (Dai et al., 2024; Patra et al., 2014; Shepherd et al., 2024; Yin et al., 2015; Zhang et al., 2006)

CO is formed due to the incomplete combustion of fossil fuels, chemical reactions when reducing iron and other minerals during extraction and processing, brick and cement production, and biomass burning (Holloway et al., 2000; Khalil and Rasmussen, 1990; Koppmann et al., 2005). Once emitted into the atmosphere, CO undergoes chemistry in-situ including oxidation into carbon dioxide (CO_2) and production from the oxidation of volatile organic compounds (VOCs) (Joshi et al.,

https://doi.org/10.5194/egusphere-2025-5890
Preprint. Discussion started: 6 January 2026

2023; Koppmann et al., 2005; World Health Organization, 2021). In unpolluted atmosphere, CO has been observed to have a higher value during local winter as the OH column is lower in winter and the mixing process is slower (Lelieveld et al., 2016; Spivakovsky et al., 2000). In industrial areas, CO has been observed to have higher values during times controlled mostly by when production is increased or efficiency of combustion is decreased (Munsif et al., 2021; Tian et al., 2022; Zhao et al., 2012). This includes during the winter when additional combustion is often found for residential heating and extra production occurs to meet end-of-year industrial deadlines (Batey, 1997; Li et al., 2025). Similarly, CO is observed to be higher locally due to when and where biomass burning occurs (Lin et al., 2020; Wang et al., 2021, 2024).

Contemporary approaches to estimating CO emissions encompass several primary technical pathways, each with distinct advantages and region-specific limitations. Bottom-up inventories combine activity data (e.g., fuel consumption, industrial production, vehicle kilometers traveled) with sector-specific emission factors, as implemented in databases such as EDGAR (Crippa et al., 2020; Olivier et al., 1999) and China's MEIC system (Zheng et al., 2018a). These inventories provide detailed sectoral and temporal information but often suffer from outdated activity data, uncertain emission factors, and incomplete representation of unregulated or diffuse sources, particularly in developing regions. Direct atmospheric observations, obtained from ground-based networks (e.g., WMO GAW stations) and satellite instruments (e.g., MOPITT, TROPOMI), offer spatially consistent and temporally continuous coverage, enabling detection of large-scale pollution events such as biomass burning (Buchholz et al., 2022; Worden et al., 2013). However, retrieval uncertainties, cloud contamination, and limited sensitivity near the surface restrict their capacity for precise emission quantification. Chemical transport model (CTM) inversions (e.g., GEOS-Chem, WRF-Chem) integrate atmospheric chemistry and dynamics to optimize emissions(Jiang et al., 2015; Kopacz et al., 2010), integrate atmospheric transport and chemistry to infer emissions from concentration fields, providing physically consistent estimates but requiring substantial computational resources and reliable prior inventories that are often unavailable in data-sparse regions. Isotopic analyses (Brenninkmeijer et al., 1999; Röckmann et al., 2002) can effectively distinguish anthropogenic and biogenic CO sources, yet their application is constrained by the need for high-precision laboratory measurements and limited spatial representativeness. Despite these methodological advances, CO emissions remain more uncertain than other well-monitored species such as CH_4, NO_2, and SO_2 (Lorente et al., 2021; Schneising et al., 2019; Wang et al., 2022; Wei et al., 2020). These challenges are particularly acute in Central Asia, where sparse monitoring, limited inventories, and heterogeneous sources—ranging from industrial activities to underground coal fires—have hindered comprehensive assessments and model validation.

Central Asia, as a core area of the Belt and Road Initiative, the emission control of its coal - intensive industries is crucial for regional air quality and trans - boundary pollution transport. Due to the rapid increase in coal use, industrial development, and economic growth, the emissions of CO is both presently not well characterized, there are few observational networks, and though to be rapidly increasing and changing (Akhmedzhanov and Karadanov, 2020; Rupakheti et al., 2021; Zeng and Shen, 2022; Zhang et al., 2011; Zhao et al., 2022). This region of the world has diverse and unique geographical and climatic conditions, environmental conditions, and development patterns, based heavily on coal and minerals (Pirajno et al., 2011; Zeng and Shen, 2022). Understanding CO emissions here is of growing importance for assessing the efficiency of coal use, especially

https://doi.org/10.5194/egusphere-2025-5890
Preprint. Discussion started: 6 January 2026

as related to non-power generating industries, as well as for industry and power production, in part due to the continued future growth expected in this area, and potential for addressing and formulating environmental and climate mitigation strategies (Action Plan for Clean and Efficient Utilization of Coal (2015-2020), 2025; Circular of the State Council on the Issuance of the Action Plan for Continuous Improvement of Air Quality).

To address these gaps, this study applies the Model-Free Inversion Estimation Framework (MFIEF)—a lightweight, mass-conserving, and observation-driven modeling system designed to infer surface CO emissions from satellite retrievals of CO and HCHO without requiring complex prior inventories or computationally intensive adjoint simulations (Li et al., 2025; Lin et al., 2020; Wang and Cohen, 2023). By explicitly accounting for satellite observational uncertainties, MFIEF provides a rapid and flexible means of estimating emissions at high spatial and temporal resolution, well suited for data-sparse and dynamically evolving regions such as Central Asia (Inness et al., 2022; Savenets et al., 2022). The framework not only enables consistent, data-driven quantification of CO emissions but also facilitates the identification of previously underrepresented or missing sources. Ultimately, the results contribute to improving emission inventories, informing mitigation policies, and advancing understanding of CO's role in regional air quality and climate interactions, with broader implications for carbon neutrality and sustainable development goals (Abduh et al., 2021; World Health Organization, 2021).

2. Data and Methods

2.1 Study Area

The study area spans from 35° N to 50° N latitude and 70° E to 100° E longitude, including parts of Xinjiang, China, Kazakhstan, Kyrgyzstan, and Uzbekistan. The climate in this region is predominantly temperate continental, including cold and dry winters and hot and arid summers, with large diurnal and annual temperature variations. The Xinjiang area has extensive coal mining as well as many industries which use the coal and are powered by the coal. In addition, coal is widely used to generate power which is then exported to areas in eastern China. This leads to significant emissions of CO and other combustion byproducts. Similarly, Kazakhstan, Kyrgyzstan, and Uzbekistan also have many industries related to energy and minerals, and also plays a crucial role in the regional CO emissions landscape. Fig. 1 illustrates the extent of the study area and the location of coal bases, power plants and steel plants within the Xinjiang region and there are eight steel plants and 105 power plants in the study area.

https://doi.org/10.5194/egusphere-2025-5890
Preprint. Discussion started: 6 January 2026

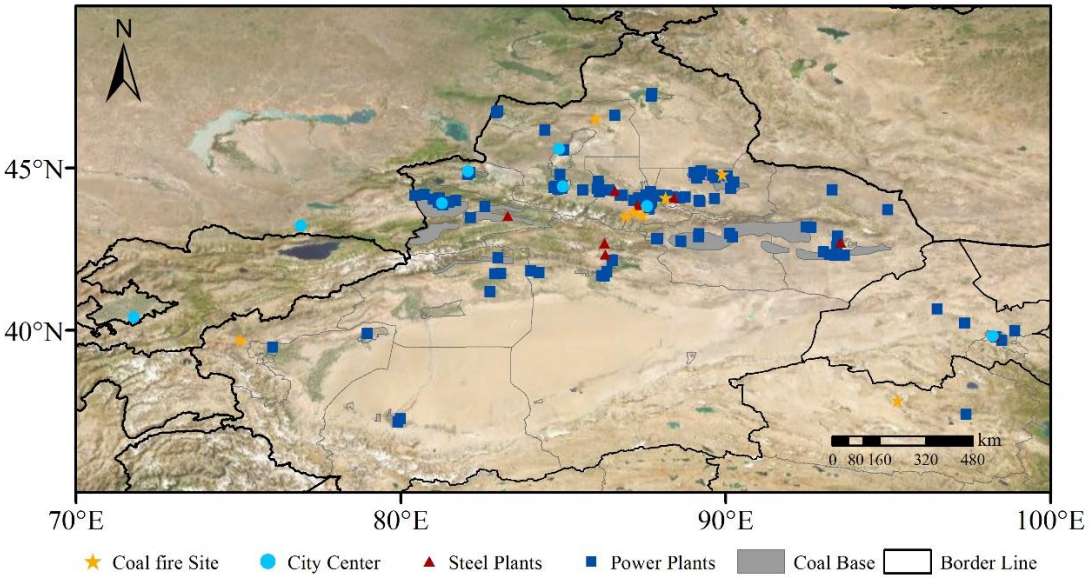

Figure 1: study area (latitude: 35° N-50° N and longitude: 70° E-100° E) and Xinjiang's major coal bases, plants.

2.2 Data

TROPOMI: The S5P (Sentinel-5 Precursor) satellite was launched in October 2017, with its sole payload being TROPOMI, a push-broom imaging spectrometer with a swath width of 2600 km (5.5 km×7 km resolution at nadir), and a local equator crossing time around 13:30, providing global coverage once daily. CO column loading is retrieved daily under both clear-sky and partially cloudy-sky conditions using the 2.3 μm spectral range of the shortwave infrared (SWIR). Clear-sky observations are sensitive to tropospheric boundary layer CO, CH_4, and aerosols, while cloudy atmospheres modify column sensitivity based on variations in the light path. Total-column averaging kernels for clear-sky and cloudy conditions provide insights into vertical sensitivity (Borsdorff et al., 2023; Landgraf et al., 2016). In this work, the Level 3 OFFL data product from Google Earth Engine (GEE) is filtered to ensure the quality assurance flag is above 0.5, and then resampled and then resampled using the Weighted Polygonal Remote Sensing Toolkit HARP (http://stcorp.github.io/harp/doc/). The data were then resampled with a resolution of 0.05°×0.05°.

HCHO is one of VOCs, and is important due to its being both directly emitted into the atmosphere by combustion, industrial activities, traffic, and fires; as well as being produced due to the chemical decay of heavier VOCs. Since the lifetime of HCHO columns is far shorter than those of CO columns, the loading of HCHO scales linearly with the rate of in-situ production of CO (Cohen and Prinn, 2011), with the decay mostly due to OH and photolysis, and as such is sensitive to the weather, climate, water availability, aerosols, and other complex atmospheric factors (Anderson et al., 2021; Dienhart et al., 2021; Lui et al., 2017).The column loading of HCHO is also successfully retrieved by TROPOMI, although its uncertainty is larger than for CO (Romahn et al., 2021). In this work, concurrent data of retrieved HCHO and CO at the same time and

https://doi.org/10.5194/egusphere-2025-5890
Preprint. Discussion started: 6 January 2026

location are used, allowing for consistency between the retrieved species. In this study, L3 HCHO data from GEE is utilized, resampled by HARP to a resolution of 0.05°×0.05°. These data can be downloaded from https://disc.gsfc.nasa.gov/datasets.

wind: ECMWF Reanalysis v5 (ERA5) data is a widely used reanalysis dataset providing high-resolution climate data, covering multiple meteorological parameters and variables (Hersbach et al., 2020). This study employs wind field products averaged at 05:00 and 06:00 Coordinated Universal Time (UTC) under the monthly mean surface pressure field. The 05:00 and 06:00 UTC times correspond to the observation periods of the TROPOMI satellite. More details can be found at https://www.ecmwf.int/en/forecasts/dataset/ecmwfreanalysis-v5.

EDGAR: The Emissions Database for Global Atmospheric Research (EDGAR) emissions database (Olivier et al., 1999) provides monthly bottom-up emissions for CO, NO_x, VOCs, and CH_4, among other species. This study specifically utilizes sectoral monthly grid data provided by the version 8.1 database, with a resolution of 0.1°×0.1°, with subsequent resampling at 0.05°×0.05°. The data cover the following key sectors: power industry, industrial combustion, buildings, transport, agriculture, fuel exploitation, industrial processes, and waste management. The data can be accessed at https://edgar.jrc.ec.europa.eu/.

AAOD： The Multi-angle Imaging Spectro Radiometer (MISR), aboard NASA's Terra satellite, is a pioneering instrument designed to characterize Earth's atmosphere and surface through simultaneous observation at nine distinct angles. A key advanced product derived from MISR data is the Absorption Aerosol Optical Depth (AAOD). This parameter quantitatively estimates the fractional optical thickness of aerosols attributable to absorption processes, primarily caused by light-absorbing species such as black carbon and mineral dust. The L3 AAOD data product used in this paper has a resolution of 0.25° and is resampled to 0.05° to distinguish dust-affected regions. The data can be searched from https://disc.gsfc.nasa.gov/datasets (Liu et al., 2025).

2.3 Research Methods

The MFIEF is utilized to estimate CO emissions (Li et al., 2023; Qin et al., 2023). Equation (2) takes into account factors such as CO column changes, chemical decay and production, and transport, and relies on retrieved data from TROPOMI CO and HCHO in order to approximation of the weighting terms of the underlying partial differential equations that govern the transformation between CO and its driving factors, using the same equations used by world-leading chemical transport models (Cohen and Prinn, 2011). Specifically, emissions cause CO to increase, acting as a source term, while chemical reactions and mixing between in-plume and out of plume regions may lead to the loss or gain of CO, and are represented by a first order linearization around the CO concentration. The transport of CO is also an important factor, affected by both pressure-induced and advective processes, with the advective term representing the horizontal movement of CO due to wind, and the pressure-induced transport term accounting for the convergence or divergence of the atmosphere itself (i.e. vertical motion). Since vertical changes do not affect inverted CO total column loadings, so instead this term accounts for the gain or loss due to non-uniform winds. As such, the transport terms can either increase or decrease the CO column in a given location depending on the direction and magnitude of the flow (Cohen et al., 2024; Li et al., 2023; Qin et al., 2023), and are related to topography, land-sea breezes, weather systems, and more. Combining these terms yields the CO emissions Eq. (1), where:

https://doi.org/10.5194/egusphere-2025-5890
Preprint. Discussion started: 6 January 2026

$$E_{CO} = \frac{dV_{CO}}{dt} + \alpha_2 \cdot V_{CO} + \alpha_3 \cdot \nabla(\boldsymbol{u} \cdot V_{CO}) - \alpha_4 \cdot V_{HCHO} \quad (1)$$

V_{CO} represents the TROPOMI CO column loading after converted the unit into (μg/m^2). $\alpha_2 \cdot V_{CO}$ represents the sink of CO with α_2(s^{-1}) as the inverse CO lifetime. $\alpha_4 \cdot V_{HCHO}$ represents CO production, with α_4(s^{-1}) as the inverse HCHO lifetime. $\nabla(\boldsymbol{u} \cdot V_{CO})$ represents the daily zonal and meridional dispersion of CO with a unit of (μg/m^2/s), and α_3(m^{-1}) represents the transport distance. This mass conservation equation for CO provides a framework for understanding and quantifying the changes in CO columns in the atmosphere, considering the various processes that influence its distribution, following (Li et al., 2025) .

The terms of this equation are initialized using this equation, TROPOMI observations and their retrieved uncertainties, meteorological data, and either an initial a priori emissions dataset, or our own previously inverted emissions dataset in the case of multiple iterations. The fitting is based on multiple least squares regression grid-by-grid on a month-by-month basis, reflecting the differences in albedo, elevation, land-surface use, emissions type, and differences in confounding variables on each pixel specifically grouping all daily data from TROPOMI and the ECMWF reanalysis where they all occur. This process provides sufficient data to compute the weighting terms, while also accounting for the changes in land-surface, atmosphere, and other factors. In the case where a pixel in any given month either does not have enough data or produces a fit with a p value larger than 0.05, the values of the model are set to NaN on that grid during that month. To ensure physically realistic and mathematically consistent values for the coefficients α_2, α_3, and α_4, physical cutoffs are applied. Any value that is not positive ($\alpha > 0$) is set to NaN.

The resulting equation is then used to calculate estimates of CO emissions and associated uncertainty across all grids when and where data exists. To estimate the maximum probability density of the coefficients during the corresponding grid-by-grid and month-by-month basis, the solution distribution of α within the valid range (from the 10th percentile to the 90th percentile of the Probability Density Function (PDF)) is sampled 1000 times per grid. The mean value of this distribution is assigned as the day's average emission in that grid, and the standard deviation is assigned as the day's average uncertainty. This process allows us to estimate the coefficients and their uncertainties, taking into account the available data and the physical constraints on the parameters, providing a more robust and accurate representation of the CO mass conservation equation in the study region.

For the calculation of CO emissions, grid point filtering based on zero-mean distribution is required. First, the emission distribution characteristics of each grid point are identified. For each grid, the distribution of its emission values is analyzed. Since random errors should behave similar to white noise, they are expected to cluster around zero mean, and have an uncertainty range roughly equally reflected by both positive and negative values. To accomplish this, we first focus on pixels with a near zero mean. Next, we find the most negative emission value -θ μg/m^2/s for each grid point and define a range from [-θ: θ] μg/m^2/s. The emission values within this range are considered to be mainly caused by noise rather than an actual emission signal. These noisy values are filtered, further eliminating pixels with large retrieval errors, and increasing confidence that the resulting inversions are valid, reliable, and robust.

https://doi.org/10.5194/egusphere-2025-5890
Preprint. Discussion started: 6 January 2026

2.4 Uncertainty

The accuracy and precision targets for TROPOMI total CO column prior to launch were 15% and 10% respectively (Landgraf et al., 2016; Martínez-Alonso et al., 2020; Veefkind et al., 2012). There hasn't been enough research on specific issues like aerosol levels, cloud cover in low cloud conditions, changes in surface reflectivity from pixel to pixel, and the initial CO and CH_4 data, which could result in greater uncertainty than what has been mentioned (Hu et al., 2024; Lu et al., 2024). The uncertainty in TROPOMI CO total column has implications for CO emission calculations. First, emission calculation relies on accurate and precise CO column concentration data. Second, since emissions estimation requires the use of a non-linear gradient operator (Cohen and Prinn, 2011), uncertainty in the spatial domain plays an additional role. Such uncertainty may propagate through the emissions equations, leading to cases where small perturbations in the observations (i.e., due to observational or retrieval uncertainty) lead to larger perturbations in inverted emissions (Beekmann and Derognat, 2003; Rao, 2005; Reilly et al., 1987) In such instances, the emissions cannot be regarded as stable; thus, their reliability is questionable. This lack of precise quantification hinders a more robust understanding of CO emissions. Therefore, it is necessary to conduct an uncertainty analysis of the observed data, and understand how it is transformed into the uncertainty of the inverted emissions products.

This work suggests perturbing the uncertainties in TROPOMI retrieved CO and HCHO column data randomly. All perturbations are randomly added to the observed data and a bootstrap is performed to sufficiently sample the uncertainty space. Specifically, each data point of CO column and HCHO column retrieved from TROPOMI, on a daily and gridded basis, has a random perturbation within the range of -10% to +10% added. In addition to the point-by-point changes, spatial changes are analyzed. For example, given two neighboring grids, if there is an overlapping portion of the data range after the random ±10% perturbations are applied, the direction of the computed gradient, and therefore the emissions may shift. In these cases, the gradient computed is likely not trustworthy, and therefore the emissions estimate is also not likely trustworthy. Specifically, the uncertainty can be expressed by Eq. (2):

$$E_{un} = (E_{CO(\pm)} - E_{CO})/E_{CO} \quad (2)$$

$E_{CO(\pm)}$ denotes the newly calculated CO emission, E_{CO} denotes the initial CO emission, E_{un} denotes the change of CO emission result, i.e., uncertainty. Other retrieved terms will behave similarly, meaning that if any of the variables behave in such a way locally across any grids on any given day, those subsets of grids may lead to a change in the net total inverted emissions which is too large, and the data ultimately not being reliable. This work adapts a conservative approach, setting any such data to NaN and discarding it from the ultimate inverted emissions products, following Zheng (2024). The CO emission calculation and data screening process flow chart is shown in Fig. 2.

https://doi.org/10.5194/egusphere-2025-5890
Preprint. Discussion started: 6 January 2026

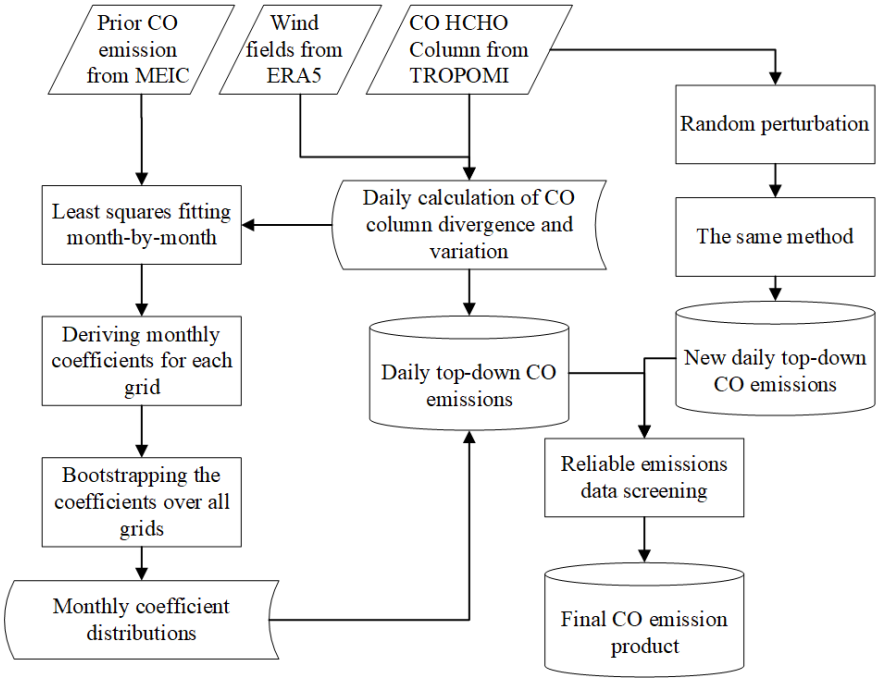

Figure 2: CO emissions calculation flowchart.

3. Results

3.1 Spatiotemporal Distribution of CO Observations

Fig. 3a presents the spatial distribution of the average TROPOMI CO total column from 2019 to 2024 across the study area, revealing a domain-wide mean of 1.54×10^{18} molec/cm^2. The concentration is predominantly influenced by anthropogenic activities, with elevated values (>2.0×10^{18} molec/cm^2) located in, around, and downwind of major urban and industrial centers such as Urumqi, Fergana, Almaty, Jiayuguan, and the Zhundong Coalfield. In contrast, natural areas like the Tianshan and Altai Mountains exhibit lower concentrations, averaging around 1.0×10^{18} molec/cm^2. Moderately high CO levels are also observed in the desert regions of central Xinjiang, likely due to enhanced photochemical production from VOCs under intense ultraviolet radiation, as well as in northwestern Kazakhstan, primarily attributable to widespread biomass incomplete combustion. The statistical distribution of the CO total column, shown in Fig. 3b, deviates from a normal distribution and is distinctly bimodal, with the 25th and 75th percentiles for the entire period calculated at 1.23 and 1.83×10^{18} molec/cm^2, respectively. Analysis of interannual variability shows that the highest CO levels occurred in 2021, with an annual mean of 1.59×10^{18} molec/cm^2, particularly in high-value zones. Conversely, 2022 marked the lowest concentrations across both high- and low-value zones, with the mean dropping to 1.44×10^{18} molec/cm^2. The values subsequently rebounded to an intermediate level in 2023 (1.52×10^{18} molec/cm^2), followed by a further increase in 2024 (1.56×10^{18} molec/cm^2). This consistent with

https://doi.org/10.5194/egusphere-2025-5890
Preprint. Discussion started: 6 January 2026

findings indicating that the general air pollution policies implemented by China are driving CO (Li et al., 2025; Liu et al., 2024) more than lockdowns related to COVID-19 (Fan et al., 2021; Zheng et al., 2021).

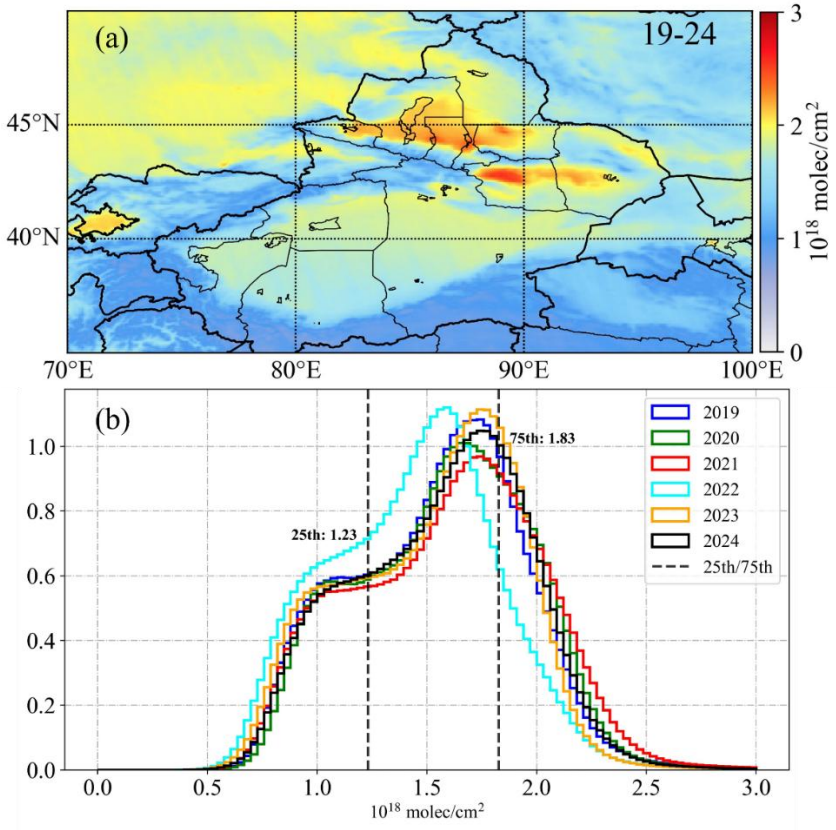

Figure 3: (a) The average of TROPOMI CO total column from 2019 to 2024; (b) PDF for 6 years.

The CO total column on a daily basis is provided in Fig. 4 for the following sites: the Wugonggou Coal Fire in Fukang, (latitude 44.075° N, longitude 88.156° E) a representative power plant, a representative steel plant, and the center of Urumqi. As observed, the CO column contains a mixture of seasonal factors (generally higher in winter and lower in summer), anthropogenic factors (generally more production near the end of the year, and additional power for heating in the coldest months including November and December), as well as some amount of random day-to-day variability. This set of findings is tied to both anthropogenic and natural forcing related to temperature, light and OH. Summer usually has more UV radiation, more OH, and less CO (Liu et al., 2022; Sun et al., 2023; Yang et al., 2021).

Among the four points in Fig. 4, the underground coal fire site, with a mean CO total column of 1.96×10^{18} molec/cm^2 and the smallest interquartile range (25^{th}-75^{th} percentile: 1.78-2.11), is primarily influenced by natural conditions and exhibits lower peak values and reduced daily variability. In contrast, the central area of Urumqi (mean: 2.18; 25^{th}-75^{th} percentile: 1.90-2.37), the steel plant (mean: 2.09; 25^{th}-75^{th} percentile:1.82-2.30), and the power plant (mean: 2.16; 25^{th}-75^{th} percentile: 1.88-2.32) are mainly affected by human activities and production demands, showing generally higher concentrations and stronger

https://doi.org/10.5194/egusphere-2025-5890
Preprint. Discussion started: 6 January 2026

variability. All four locations display seasonal fluctuations with clear peaks and troughs. Statistically, emissions from the power plant closely resemble those in central Urumqi ($R^2 = 0.55$, $p < 0.001$, RMSE = 0.30×10^{18} molec/cm²), while the Wugonggou Coal Fire site aligns more closely with the steel plant ($R^2 = 0.35$, $p < 0.001$, RMSE = 0.33×10^{18} molec/cm²). These distinctions in both concentration levels and temporal behavior suggest that different types of emission sources can be identified based on their varying seasonal patterns and trends.

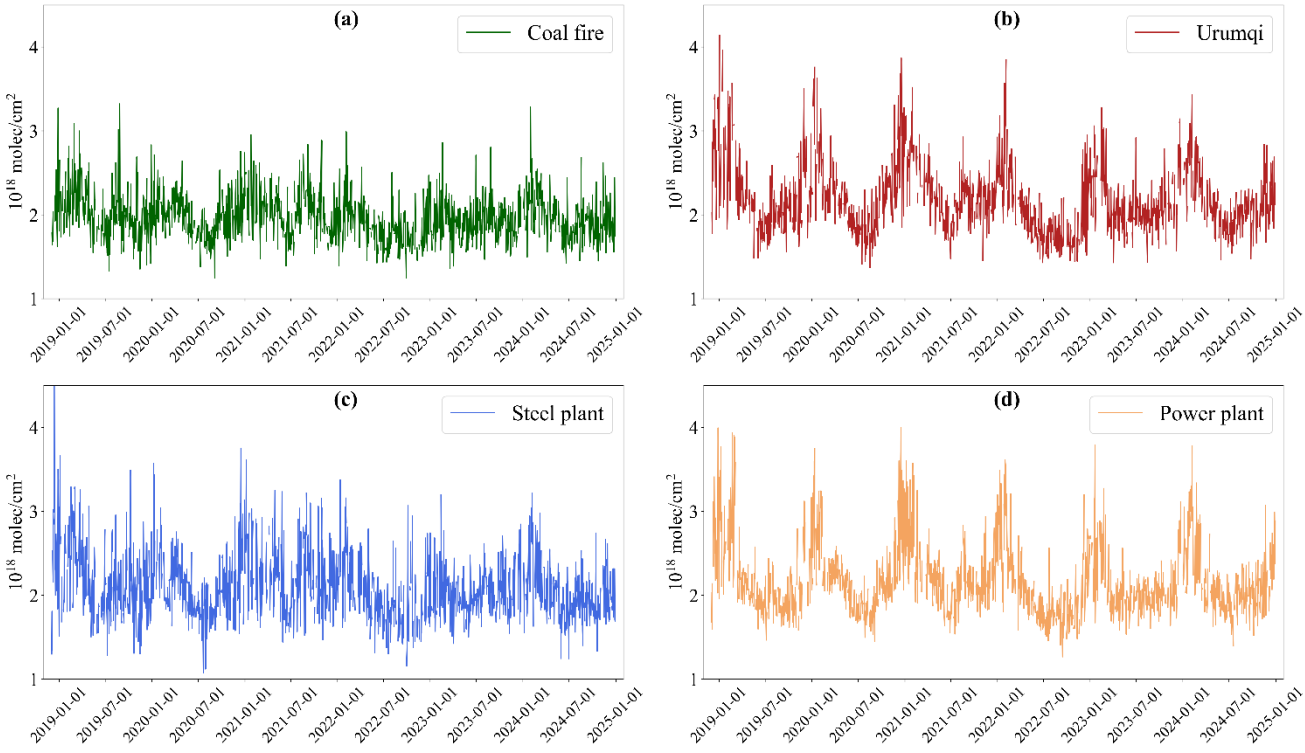

Figure 4: Time series of TROPOMI CO column for (a) coal fire site; (b) Urumqi city center (c) steel plant; and (d) power plant.

3.2 Spatiotemporal Distribution of CO Emissions

To distinguish dust-dominated regions from other aerosol types, we utilized the AAOD ratio between 443 nm and 880 nm. Mineral dust typically exhibits stronger absorption at shorter wavelengths due to its iron oxide content, leading to higher $AAOD_{443}/AAOD_{880}$ ratios, whereas other aerosols like black carbon show less spectral dependence. A higher ratio thus suggests a greater contribution of dust to total absorption. Based on this spectral behavior, we selected a threshold of $AAOD_{443}/AAOD_{880} > 4.5$ to identify and mask dust-dominated areas, thereby minimizing potential biases in CO emission estimates associated with dust contamination. Grid cells exceeding this threshold were excluded, effectively removing spurious emission signals caused by high surface reflectivity in arid regions. As shown in Fig. 5a, the spatial distribution of AAOD ratios highlights extensive dust-affected areas, primarily in the desert and arid parts of western China and southern Kazakhstan.

https://doi.org/10.5194/egusphere-2025-5890
Preprint. Discussion started: 6 January 2026

This screening process resulted in the exclusion of approximately 14% of the study area, underscoring the importance of aerosol correction in satellite-based emission inversion.

To evaluate the impact of input data uncertainty on emission estimates, we performed a perturbation analysis by varying the total column concentrations of CO and HCHO within ranges of ±10% and ±20%, reflecting uncertainties from TROPOMI retrievals and model inputs. Grid cells were classified as having "reliable emissions" only if the relative variation in estimated emissions remained within the corresponding threshold. As illustrated in Fig. 5b, under the ±10% and ±20% uncertainty thresholds, 31.3% and 33.7% of grid cells, respectively, met the reliability criterion over the six-year period. Furthermore, Fig. 5c shows the number of days with reliable emissions after applying the ±10% filter, with a spatial average of approximately 135 days per grid cell. The results indicate that stricter uncertainty filtering leads to a gradual reduction in credible emission estimates, highlighting the sensitivity of inversion outcomes to uncertainties in the input column concentrations.

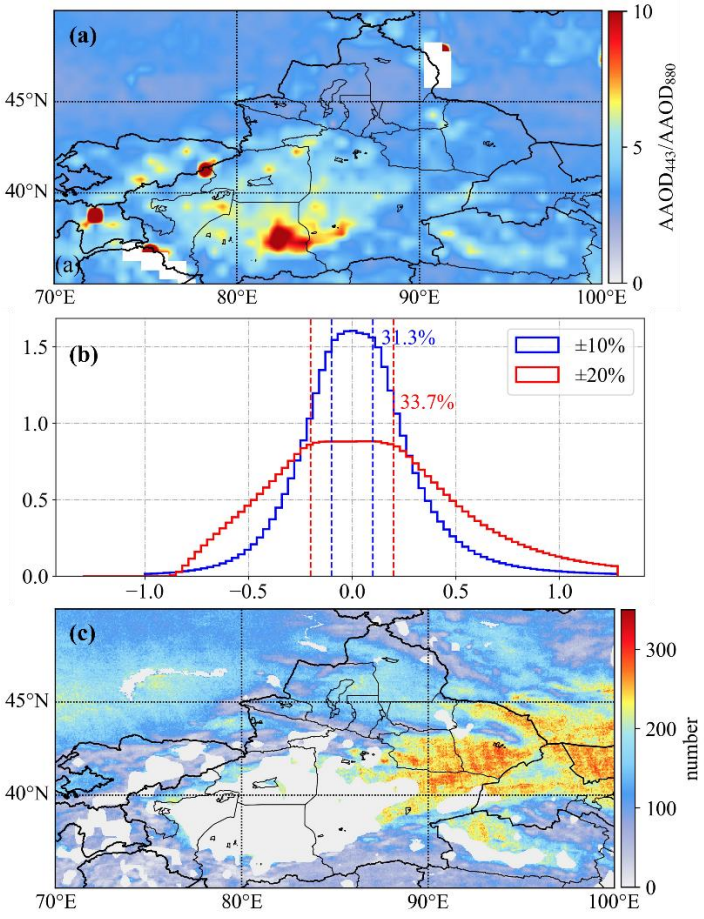

Figure 5: (a) $AAOD_{443}/AAOD_{880}$ Ratio; (b)Plausible CO emission share with perturbation added to both CO and HCHO columns; and (c) number of credible data in uncertainty calculations.

https://doi.org/10.5194/egusphere-2025-5890
Preprint. Discussion started: 6 January 2026

Following the application of a ±10% uncertainty filter, the spatial pattern of CO emissions was found to be consistent with that of the CO total column, though significant interannual variability was observed. As shown in Fig. 6, a pronounced decreasing trend from 2019 to 2024 is demonstrated by the contraction of emission hotspots in the spatial distribution (a), a systematic leftward shift of the probability distribution toward lower values (b), and a marked reduction in spatial variability reflected in the standard deviation distribution (c).

The annual mean CO concentration in the study area has been substantially declined, from 4.93 μg/m^2/s in 2019 to 3.06 μg/m^2/s in 2024, with a reduction of approximately 38%. This overall trend toward lower emissions is further reflected in the evolution of emission hotspots, which are defined as regions where the concentration is exceeded twice the study area's mean (6.72 μg/m^2/s). A total of 11 such hotspots were identified, primarily situated between 39.83°-46.58°N and 81.08°-98.23°E. Their average intensity decreased markedly from 9.51 μg/m^2/s in 2019 to 5.63μg/m^2/s in 2024, representing a total reduction of 40.8% or an average annual decrease of 0.68 μg/m^2/s. The PDFs of the emissions (Fig. 6b) provide further evidence of this systematic reduction, showing a distinct leftward shift toward lower values. The distribution peak decreased from 3.34 μg/m^2/s in 2019 to 2.85 μg/m^2/s in 2024, while the mean emission fell from 4.47 μg/m^2/s to 3.17 μg/m^2/s. Concurrently, the PDFs of the standard deviations (Fig. 6c) indicate a significant weakening of spatial heterogeneity, with the peak value dropping from 1.66 μg/m^2/s to below 1.30 μg/m^2/s. In summary, the results depicted in Fig. 6 clearly highlight a marked downward trend in CO emissions between 2019 and 2024, characterized by a contraction and weakening of emission hotspots, a systematic shift of the emission distribution to lower values, and reduced spatial variability. These observed changes are likely attributable to the combined effects of implemented emission control policies, ongoing industrial restructuring, and shifts in regional energy consumption patterns.

https://doi.org/10.5194/egusphere-2025-5890
Preprint. Discussion started: 6 January 2026

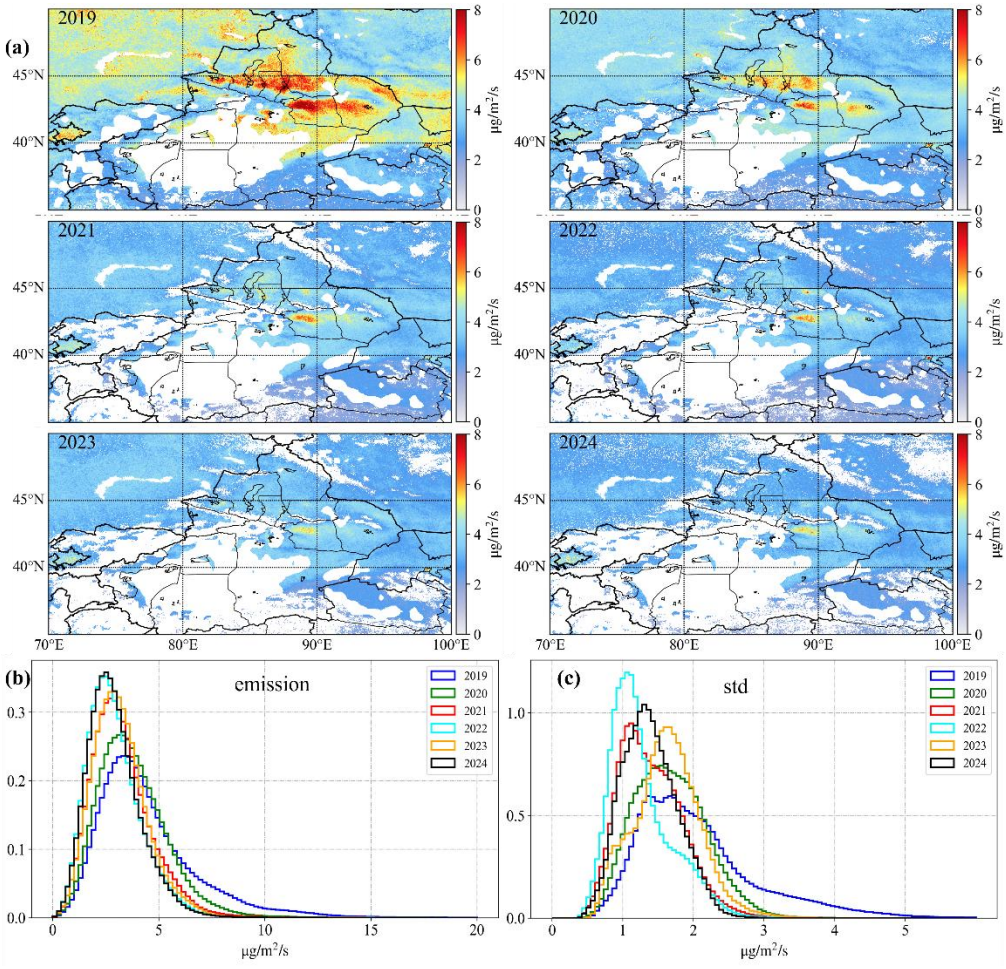

Figure 6: (a)Annual mean of CO emissions, excluding all locations which have fewer than 10 days of successfully retrieved CO emissions; (b) PDF of CO emissions for each year (c) PDF of standard deviations for every year.

Fig.7 presents the monthly variations of average CO emissions and the corresponding number of valid observational days over the study region during December 2018-December 2024. Overall, CO emissions exhibited a clear downward trend, decreasing from an exceptionally high level of 9.25 μg/m^2/s in January 2019 to around 2.5-3.0 μg/m^2/s after 2022, with occasional wintertime rebounds (e.g., 5.07 μg/m^2/s in December 2023). Seasonal fluctuations are evident, with higher emissions generally observed in winter and early spring, and lower values during late spring and summer, consistent with stronger heating-related combustion sources in cold seasons and enhanced atmospheric dispersion in warmer months. The number of valid observational days shows substantial variability, ranging from fewer than 2 days per month (e.g., July 2020 and August 2022-2024) to more than 5 days per month (December 2021). Despite this variability, the temporal patterns of emissions are robust and not simply driven by observation coverage. The joint evolution of these two metrics highlights both the long-term decline in regional CO emissions and the persistence of seasonal emission peaks, which together reflect the combined influences of anthropogenic activity, energy use, and atmospheric conditions across Xinjiang and Central Asia.

https://doi.org/10.5194/egusphere-2025-5890
Preprint. Discussion started: 6 January 2026

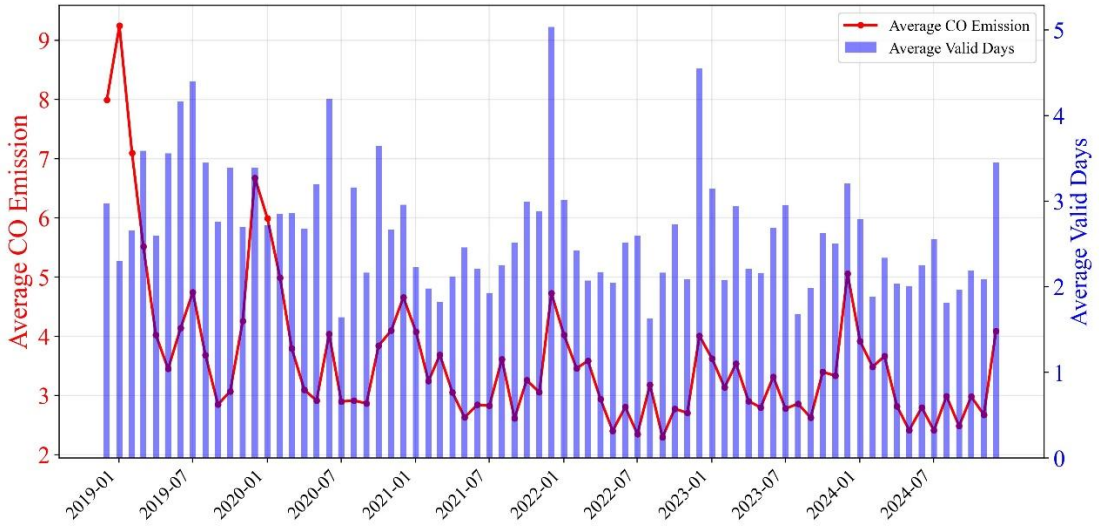

Figure 7: Average CO emissions and average valid Days per grid, per month, over the region.

Fig. 8 illustrates the temporal evolution of CO emissions from four representative point sources, namely the Wugonggou Coal Fire site, Urumqi city center, a steel plant, and a power plant. The coal fire site shows an average emission of 4.56 μg/m^2/s, with peak values exceeding 14.0 μg/m^2/s in 2019, but a significant long-term decline (trend slope = -0.78 μg/m^2/s per year). Strong seasonality is evident, with emissions nearly tripling in winter (December – January: ~8.4 μg/m^2/s) compared to summer months (<3.5 μg/m^2/s). In contrast, Urumqi exhibits the highest variability, with an overall mean of 5.14 μg/m^2/s but extreme peaks reaching 17.33 μg/m^2/s in December 2018. The city center also shows the steepest downward trend (slope = -1.32 μg/m^2/s per year), reflecting both stringent emission controls and seasonal heating demand. Wintertime (December - January) emissions are consistently elevated (~9-11 μg/m^2/s), highlighting the influence of residential heating and traffic-related combustion. The steel plant records a similar mean level (5.27 μg/m^2/s), but with more frequent high-emission episodes (20 exceedances above 8.3 μg/m^2/s), particularly in 2018-2019 when values exceeded 16 μg/m^2/s. Despite subsequent reductions, moderate seasonal peaks persist in late autumn and winter, suggesting the role of industrial production cycles. Finally, the power plant exhibits the highest average emissions (5.37 μg/m^2/s) among the four sites, with peaks above 15 μg/m^2/s in December 2018. Although emissions have gradually declined (slope = -0.92 μg/m^2/s per year), strong winter enhancements remain (December average: 8.36 μg/m^2/s), consistent with increased electricity and heating demand. Overall, all four sources demonstrate a common pattern of pronounced winter peaks and declining interannual trends, but with varying magnitudes and persistence. These results emphasize the combined impact of seasonal energy consumption, urban activity, and industrial operations on localized CO emission dynamics across Xinjiang.

https://doi.org/10.5194/egusphere-2025-5890
Preprint. Discussion started: 6 January 2026

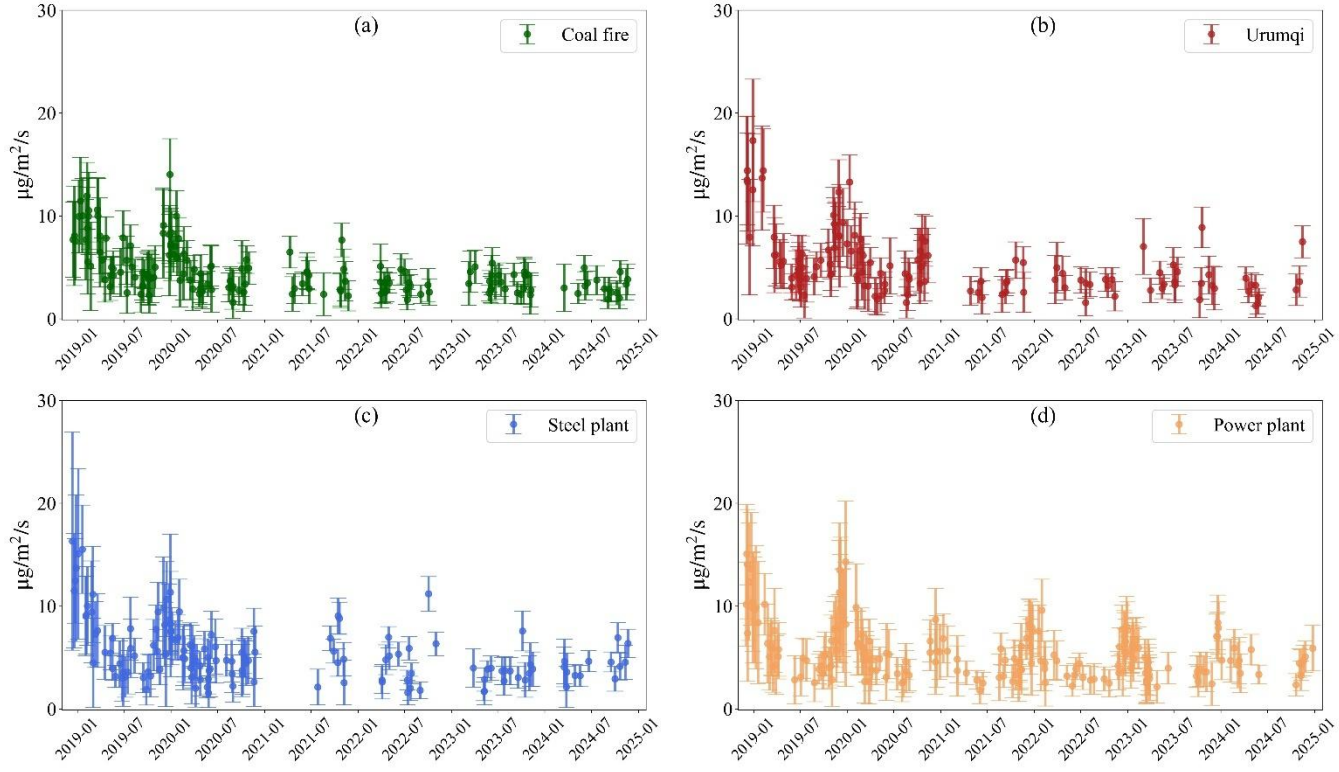

Figure 8: CO emissions of (a) Wugonggou Coal Fire site; (b) Urumqi city center; (c) steel plant; and (d) power plant.

From Table 1, all four point source categories show a consistent downward trend in CO emissions from 2019 to 2024. The most pronounced reduction occurred at the power plants, where the mean value dropped from 6.45 to 3.76 μg/m² /s, a decrease of 42%. Substantial declines are also observed at the coal fire site and the steel plants; the former decreased from 5.08 to 3.10 μg/m² /s (-39%), and the latter from 6.81 to 4.36 μg/m² /s (-36%). In comparison, the city center site recorded the smallest relative reduction, with its mean value falling from 6.44 to 4.17 μg/m² /s (-35%). This trend is even more evident in the upper percentiles. The 90th percentile value for power plants fell sharply from 11.77 μg/m² /s in 2019 to 5.95 μg/m² /s in 2024, while the steel plants saw a decrease from 11.87 μg/m² /s to 7.36 μg/m² /s over the same period. This indicates a significant control over high-emission episodes across all categories, particularly at the industrial facilities. Overall, the data demonstrates effective emission mitigation across all categories during this period, with power plants and the coal fire site achieving the largest relative decreases.

https://doi.org/10.5194/egusphere-2025-5890
Preprint. Discussion started: 6 January 2026

Table 1: Percentile of CO emission data for four types of points (City Center, Coal fire site, Steel Plants and Power Plants) from 2019-2024 and the Change rate (unit: μg/m²/s).

type	Year	Mean	10th	20th	50th	80th	90th	Rate
City Center	2019	6.44	3.09	3.83	5.50	9.04	11.12	
	2020	5.10	2.43	3.05	4.39	6.75	8.48	-21%
	2021	4.37	2.32	2.75	3.79	5.55	7.48	-14%
	2022	4.43	1.85	2.26	3.63	5.67	8.33	1%
	2023	4.47	2.36	2.81	3.95	5.94	7.38	1%
	2024	4.17	2.08	2.57	3.51	5.34	6.61	-7%
Coal fire site	2019	5.08	2.45	2.93	4.42	6.91	8.33	
	2020	4.27	2.25	2.77	3.95	5.59	6.80	-16%
	2021	3.38	1.85	2.31	3.16	4.38	5.22	-21%
	2022	3.09	1.64	1.90	2.87	4.08	4.78	-9%
	2023	3.30	1.89	2.35	2.99	4.30	4.79	7%
	2024	3.10	1.73	2.01	2.93	4.14	4.70	-6%
Steel plants	2019	6.81	3.04	3.75	5.64	9.45	11.87	
	2020	5.53	2.79	3.42	5.01	7.07	9.52	-19%
	2021	4.96	2.61	3.27	4.50	6.51	7.78	-10%
	2022	5.12	2.07	2.73	4.56	6.80	8.39	3%
	2023	4.82	2.58	3.03	4.29	6.47	8.02	-6%
	2024	4.36	2.00	2.36	3.93	6.06	7.36	-9%
Power plants	2019	6.45	2.91	3.54	5.31	9.00	11.77	
	2020	5.29	2.65	3.22	4.77	6.94	8.76	-18%
	2021	4.40	2.28	2.81	4.02	5.76	7.00	-17%
	2022	4.02	2.04	2.50	3.61	5.31	6.41	-9%
	2023	3.97	2.16	2.67	3.75	5.12	6.03	-1%
	2024	3.76	2.00	2.42	3.44	4.85	5.95	-5%

To evaluate the consistency of the inverted CO emissions with actual fuel usage, we collected official data on annual coal consumption for several major power plants within the study area for the year 2023. As shown in Table 2, coal consumption per plant varied from about 57,070 to 205,440 tons, with corresponding estimated CO emissions ranging from approximately 1,675 to 6,426 tons. The derived emission factors (EF), defined as the ratio of CO emissions to coal consumed (EF = CO emissions / coal consumption), vary between 0.9% and 7.7%. Larger facilities such as Ganquanbao TBEA, Huadian Urumqi, Huaneng Fukang Industrial Park, and Tianchi Changji Cogen generally exhibit lower EFs, ranging from 0.9% to 2.9%, suggesting higher combustion efficiency and effective emission control. In contrast, smaller or industrially associated plants, including Urumqi Petrochemical, Xinjiang Joinworld, and Xinjiang Zhongtai Fukang, show higher EFs, between 2.9% and 7.7%, which may reflect variations in coal quality, boiler technology, or combustion conditions. Overall, these emission factors align well with typical ranges for CO from coal combustion reported in established bottom-up inventories such as EDGAR

https://doi.org/10.5194/egusphere-2025-5890
Preprint. Discussion started: 6 January 2026

and MEIC. The coherence between reported fuel use and satellite-derived emissions supports the reliability of the inversion methodology, particularly in regions with limited ground-based monitoring.

Table 2: Annual coal consumption and CO emissions of 12 power plants in 2023

Name	Latitude	Longitude	Tons of Coal (2023)	Tons of CO (2023)10th	Tons of CO (2023)90th	EF (10th -90th)
Huadian Urumqi power station	43.901111	87.6975	188320	2098	4265	1.1%-2.3%
Xinjiang Joinworld power station	43.914734	87.583101	85600	2258	4311	2.6%-5.0%
Xinjiang Zhongtai Huatai power station	43.942935	87.664081	85600	2098	4265	2.5%-5.0%
Urumqi Petrochemical power station	43.970245	87.721928	57070	1675	4367	2.9%-7.7%
Tianchi Changji Cogen power station	44.004362	87.171961	199740	1865	4229	0.9%-2.1%
Huadian Changji power station	44.06325	87.326558	188320	1936	5754	1.0%-3.1%
Xinjiang Zhongtai Fukang power station	44.08098	88.588901	85600	1742	4832	2.0%-5.6%
Tianlong Mining Fukang Smelting power station	44.099778	88.373315	114140	1746	3904	1.5%-3.4%
Ganquanbao TBEA power station	44.124707	87.770718	199740	2025	5727	1.0%-2.9%
Huaneng Fukang Industrial Park power station	44.133333	87.933333	199740	1886	4512	0.9%-2.3%
Shenhua Guoneng Fukang power station	44.13336	87.834665	85600	2075	5084	2.4%-5.9%
Wujiaqu power station	44.26892	87.687877	205440	2574	6426	1.3%-3.1%

4. Discussion

A comparison between this emission and EDGAR is presented in Fig. 9a, illustrating the spatial distribution of the mean CO emissions in the study area for the period from 2019 to 2022, during which it can be observed that the high emission values are mainly concentrated in urban and industrialized regions in northern Xinjiang, as well as in some regions of Kazakhstan, which may have high CO emissions due to industrial activities, transportation and home heating. In contrast, low emission values are mainly found in remote areas of Xinjiang, such as steppes, deserts, and mountainous regions, as well as in some sparsely populated and less industrialized regions of Kazakhstan. Overall, the geographical distribution of CO emissions shows obvious unevenness, with the emission intensity in urban and industrial areas being significantly higher than that in the surrounding rural and natural areas, especially in the urban agglomerations in northern Xinjiang and some industrial areas in Kazakhstan, where high emissions may be related to the local level of economic development, the structure of energy consumption, and the industrial layout. Fig. 9b shows the mean difference between

https://doi.org/10.5194/egusphere-2025-5890
Preprint. Discussion started: 6 January 2026

the CO emissions estimated in this study and the EDGAR emission inventory across the study area from 2019 to 2022. While the emissions from this study are higher than EDGAR in most regions, urban centers such as Urumqi and Almaty show the opposite trend, with values up to 5 μg/m²/s lower than EDGAR. In the figure, the blue areas of the figure are mainly distributed. Madrazo et al (2018) compared local Cuban emission inventories with EDGAR for CO emissions and mentioned that EDGAR overestimates the stationary source emission factors by a factor of three, while Li et al (2025) indicates that both EDGAR and MEIC estimates of well-established urban areas and large factories overestimate CO emissions in Shanxi, while newer and smaller urban sources are underestimated or missing. Fig.9(c) shows the PDF of the differences between our CO emission estimates and the EDGAR inventory over the study region. Across 2019-2022, the differences are predominantly positive, with 99.9% of grid points showing higher emissions in our estimates. The annual mean and median differences gradually decrease from 3.95 and 3.64 μg/m²/s in 2019 to 2.50 and 2.43 μg/m²/s in 2022, indicating a narrowing gap over time. The PDF peaks shift similarly from 3.20 μg/m²/s in 2019 to 2.20 μg/m²/s in 2022, while the overall range remains largely positive. These statistics suggest that our inversion generally yields higher CO emissions than EDGAR, with differences decreasing over time and concentrated in high-emission areas.

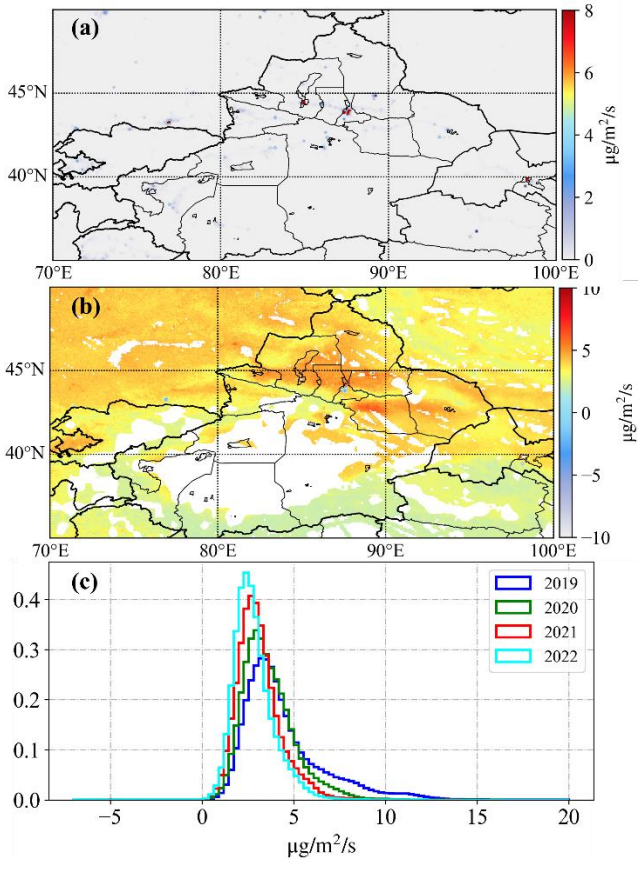

Figure 9: (a) EDGAR CO emissions; and (b) difference between this study's results and EDGAR; and (c) monthly difference PDF.

https://doi.org/10.5194/egusphere-2025-5890
Preprint. Discussion started: 6 January 2026

A fundamental methodological divergence between satellite observations and model-based inventories is demonstrated in Fig.10. At four confirmed coal fire sites, TROPOMI unambiguously detects strong CO emission, whereas the EDGAR inventory shows negligible emissions. This discrepancy arises because the bottom-up EDGAR inventory, by design, excludes non-industrial sources such as coal fires. Furthermore, the comparison in urban regions (e.g., Urumqi, Almaty) reveals a pattern of partial agreement and quantitative divergence. While the datasets show consistent temporal trends, EDGAR exhibits systematic biases, overestimating winter peaks in some cities and displaying spatial inaccuracies in others. These discrepancies are attributable to limitations in the inventory's activity data, the regional applicability of its emission factors, and its coarse spatial resolution.

Collectively, these findings underscore the value of top-down satellite data. This approach not only identifies emission sources missing from conventional inventories but also provides an independent means for validating urban emission estimates, proving indispensable for developing accurate global carbon budgets and targeted climate policies.

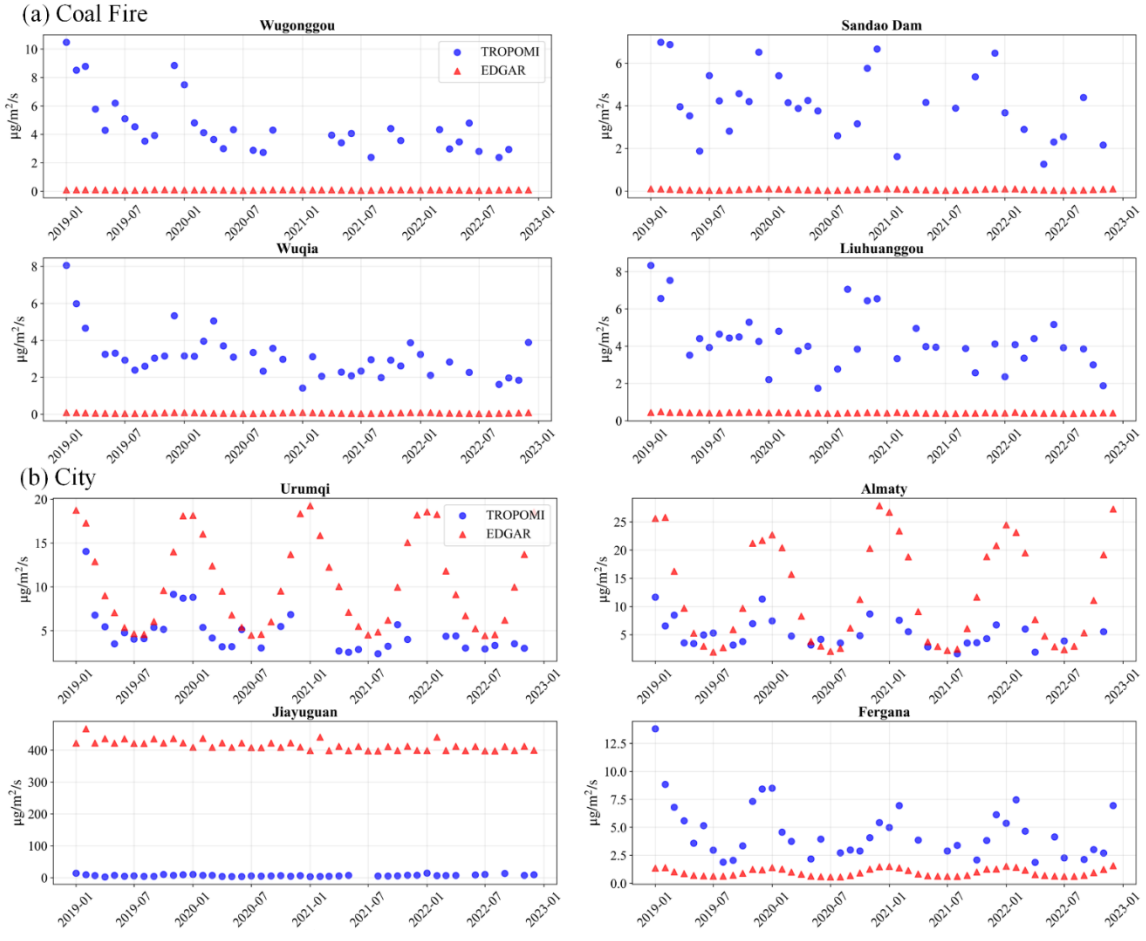

Figure 10: Comparison of CO Emission Fluxes from TROPOMI Observations and EDGAR Inventory at (a) Coal Fire Sites; and (b) Urban Centers.

https://doi.org/10.5194/egusphere-2025-5890
Preprint. Discussion started: 6 January 2026

5. Conclusion

In this study, we applied the MFIEF to quantify CO emissions across Central Asia by integrating TROPOMI CO and HCHO retrievals with meteorological reanalysis data. By explicitly accounting for satellite observational uncertainties, our approach provides a more reliable representation of emission dynamics in a region where ground-based measurements and inventory data remain scarce. This is especially important in this region of the world, where the economic growth is very large and industries and urban areas are both expanding rapidly. Furthermore, there is rapid development of both the chemical industry due to the production of many rare earths in this area, coupled with the rapid implementation of solar and wind power, all of which leads to substantial CO emissions during the production process.

The results reveal a pronounced interannual decline of approximately 38% in CO emissions from 2019 to 2024, indicating that although not directly targeted by various emissions rules and regulations, that it is never the less being mitigated as a co-emitted substance along with targeted species. Furthermore, distinct seasonal variations are observed with stronger emissions during winter and early spring, reflecting increases in energy demand through the colder periods of the year, industrial production increases in the lead up to the Chinese New Year, and local meteorological influences in part due to the unique snow and desert environment. Attribution analysis further highlights the contribution of major industrial centers, power plants, and urban agglomerations, while also pointing to previously underrepresented sources such as underground coal fires. Comparison with the commonly used EDGAR emissions database underscores both the limitations of global inventories in capturing local emission characteristics and the value of satellite-based approaches for identifying missing or mischaracterized sources.

Beyond providing an updated regional emission assessment, this work demonstrates the critical importance of explicitly treating observational uncertainties, which contribute substantially to the fact that about 69% of grids are found to not have sufficiently reliable CO retrievals to be useful for successful emissions inversion. This study advances the understanding of CO emissions in Central Asia by integrating TROPOMI observations with the MFIEF framework and explicitly computing both emissions uncertainties, as well as regions when and where emissions cannot be reliably inverted. The results not only provide valuable constraints for regional inventories and emission source characterization but also strengthen the foundation for retrieving CH_4, CO_2, and other SWIR- and NIR-absorbing species. Beyond regional relevance, the approach offers broader implications for improving bottom-up inventories, supporting air quality modeling, and informing climate and carbon mitigation strategies.

Limitations of the current work come from three different directions. First, there are no on-the-ground or direct observations of emissions from CEMS or other networks for CO, although such observations do exist for NO_x and SO_2 and may be possible to be scaled. Second, the observational uncertainty in this work is based on the column values of retrieved CO, and the issue of the vertical distribution has not been considered. This is also true in part because of the lack of vertical observations in this part of the world. Finally, due to the rapid growth of the economy on the ground, there may be assumptions which were made in terms of surface albedo or land-use type which are already outdated in terms of updating the algorithms

https://doi.org/10.5194/egusphere-2025-5890
Preprint. Discussion started: 6 January 2026

of the satellite retrieval themselves. This is highlighted by the identified substantial underground coal fire, which emits a large amount of CO while at the same time emitting a large amount of absorbing aerosol. Since the a priori used to invert the satellite retrieval did not contain this information, it is possible that there is some bias in the retrieved column values, in addition to the uncertainties posed, providing additional insights for future work.

Data availability

The authors would like to thank the TROPOMI, ERA-5, and EDGAR products for making their data available. The satellite CO and HCHO datasets used in this study are available at https://disc.gsfc.nasa.gov/datasets. The ERA-5 reanalysis product is available at https://doi.org/10.24381/cds.bd0915c6. The EDGAR product can be accessed from https://edgar.jrc.ec.europa.eu/. The data that support the findings of this study are openly available at the following URL/DOI: https://doi.org/10.6084/m9.figshare.28462817.

Author contribution

This work was conceptualized by Jason Blake Cohen and Ye Feng. The methods were developed by Jason Blake Cohen and Kai Qin. Xiaolu Li and Lingxiao Lu provided insights on methodology. Visualizations were made by Ye Feng and Jason Blake Cohen. Writing of the original draft was done by Ye Feng and Jason Blake Cohen. Writing at the review and editing stages were done by Xiaolu Li, Lingxiao Lu, Zhewen Liu, Lei Wang, Jian Liu and Jason Blake Cohen.

Competing Interests

At least one of the (co-)authors is a member of the editorial board of Atmospheric Chemistry and Physics.

Acknowledgments

This research was supported by the Natural Science Foundation of Jiangsu Province (Grants No BKBZ2024060).

https://doi.org/10.5194/egusphere-2025-5890
Preprint. Discussion started: 6 January 2026

Reference

Abduh, N., Muhibuddin, A., Zulkarnain, Z., Yusuf, R., and Buraerah, F.: Carbon monoxide gas pollution control model using reducing plants, J. Environ. Treat. Tech., 9, 428–34, https://doi.org/10.47277/JETT/9(2)434, 2021.

Adams, S., Boateng, E., and Acheampong, A. O.: Transport energy consumption and environmental quality: does urbanization matter?, Sci. Total Environ., 744, 140617, https://doi.org/10.1016/j.scitotenv.2020.140617, 2020.

Akhmedzhanov, A. Kh. and Karadanov, T. K.: Atmospheric Carbon Dioxide Dynamics over Kazakhstan Derived from Satellite Data, Russ. Meteorol. Hydrol., 45, 54–57, https://doi.org/10.3103/S1068373920010070, 2020.

Anderson, D. C., Duncan, B. N., Fiore, A. M., Baublitz, C. B., Follette-Cook, M. B., Nicely, J. M., and Wolfe, G. M.: Spatial and temporal variability in the hydroxyl (OH) radical: understanding the role of large-scale climate features and their influence on OH through its dynamical and photochemical drivers, Atmospheric Chem. Phys., 21, 6481–6508, https://doi.org/10.5194/acp-21-6481-2021, 2021.

Batey, J.: An overview of carbon monoxide generation and release by home appliances, Brookhaven National Lab. (BNL), Upton, NY (United States), 1997.

Beekmann, M. and Derognat, C.: Monte Carlo uncertainty analysis of a regional-scale transport chemistry model constrained by measurements from the Atmospheric Pollution Over the Paris Area (ESQUIF) campaign, J. Geophys. Res. Atmospheres, 108, https://doi.org/10.1029/2003JD003391, 2003.

Bel, G. and Holst, M. %J T. P.: Evaluation of the impact of bus rapid transit on air pollution in Mexico City, Transp. Policy, 63, 209–220, https://doi.org/10.1016/j.tranpol.2018.01.001, 2018.

Borsdorff, T., aan de Brugh, J., Pandey, S., Hasekamp, O., Aben, I., Houweling, S., and Landgraf, J.: Carbon monoxide air pollution on sub-city scales and along arterial roads detected by the Tropospheric Monitoring Instrument, Atmospheric Chem. Phys., 19, 3579–3588, https://doi.org/10.5194/acp-19-3579-2019, 2019.

Borsdorff, T., Campos, T., Kille, N., Volkamer, R., and Landgraf, J.: Vertical information of CO from TROPOMI total column measurements in context of the CAMS-IFS data assimilation scheme, Atmospheric Meas. Tech. Discuss., 2022, 1–20, 2022.

Borsdorff, T., Landgraf, J., and Sha, M. K.: TROPOMI Carbon Monoxide, in: Handbook of Air Quality and Climate Change, edited by: Akimoto, H. and Tanimoto, H., Springer Nature Singapore, Singapore, 261–270, https://doi.org/10.1007/978-981-15-2760-9_59, 2023.

Brenninkmeijer, C. A. M., Röckmann, T., Bräunlich, M., Jöckel, P., and Bergamaschi, P.: Review of progress in isotope studies of atmospheric carbon monoxide, Chemosphere-Glob. Change Sci., 1, 33–52, https://doi.org/10.1016/S1465-9972(99)00018-5, 1999.

Brioude, J., Angevine, W. M., Ahmadov, R., Kim, S.-W., Evan, S., McKeen, S. A., Hsie, E.-Y., Frost, G. J., Neuman, J. A., and Pollack, I. B.: Top-down estimate of surface flux in the Los Angeles Basin using a mesoscale inverse modeling technique: assessing anthropogenic emissions of CO, NO x and CO 2 and their impacts, Atmospheric Chem. Phys., 13, 3661–3677, https://doi.org/10.5194/acp-13-3661-2013, 2013.

Buchholz, R. R., Park, M., Worden, H. M., Tang, W., Edwards, D. P., Gaubert, B., Deeter, M. N., Sullivan, T., Ru, M., and Chin, M.: New seasonal pattern of pollution emerges from changing North American wildfires, Nat. Commun., 13, 2043, https://doi.org/10.1038/s41467-022-29623-8, 2022.

Cohen, J., Li, X., Tiwari, P., Wu, L., Wang, S., He, Q., Yang, H., and Qin, K.: Space-based inversion tracks and attributes Shanxi's under-estimated carbon monoxide emissions, https://doi.org/10.21203/rs.3.rs-4604393/v1, 17 July 2024.

Cohen, J. B. and Prinn, R. G.: Development of a fast, urban chemistry metamodel for inclusion in global models, Atmospheric Chem. Phys., 11, 7629–7656, https://doi.org/10.5194/acp-11-7629-2011, 2011.

Crippa, M., Solazzo, E., Huang, G., Guizzardi, D., Koffi, E., Muntean, M., Schieberle, C., Friedrich, R., and Janssens-Maenhout, G.: High resolution temporal profiles in the Emissions Database for Global Atmospheric Research, Sci. Data, 7, 121, https://doi.org/10.1038/s41597-020-0462-2, 2020.

Dai, M., Niu, Q., Wu, S., Lin, Y., Biswas, J. K., and Yang, C.: Hydroxyl radicals in ozone-based advanced oxidation of organic contaminants: A review, Environ. Chem. Lett., 22, 3059–3106, https://doi.org/10.1007/s10311-024-01772-w, 2024.

Dienhart, D., Crowley, J. N., Bourtsoukidis, E., Edtbauer, A., Eger, P. G., Ernle, L., Harder, H., Hottmann, B., Martinez, M., Parchatka, U., Paris, J.-D., Pfannerstill, E. Y., Rohloff, R., Schuladen, J., Stönner, C., Tadic, I., Tauer, S., Wang, N., Williams, J., Lelieveld, J., and Fischer, H.: Measurement report: Observation-based formaldehyde production rates and

https://doi.org/10.5194/egusphere-2025-5890
Preprint. Discussion started: 6 January 2026

their relation to OH reactivity around the Arabian Peninsula, Atmospheric Chem. Phys., 21, 17373–17388, https://doi.org/10.5194/acp-21-17373-2021, 2021.

Sentinel-5 precursor/TROPOMI Level 2 Product User Manual Formaldehyde HCHO:

Fan, H., Wang, Y., Zhao, C., Yang, Y., Yang, X., Sun, Y., and Jiang, S.: The Role of Primary Emission and Transboundary Transport in the Air Quality Changes During and After the COVID-19 Lockdown in China, Geophys. Res. Lett., 48, e2020GL091065, https://doi.org/10.1029/2020GL091065, 2021.

Fortems-Cheiney, A., Chevallier, F., Pison, I., Bousquet, P., Szopa, S., Deeter, M. N., and Clerbaux, C.: Ten years of CO emissions as seen from Measurements of Pollution in the Troposphere (MOPITT), J. Geophys. Res. Atmospheres, 116, https://doi.org/10.1029/2010JD014416, 2011.

Hanaoka, T. and Masui, T. %J E. P.: Exploring effective short-lived climate pollutant mitigation scenarios by considering synergies and trade-offs of combinations of air pollutant measures and low carbon measures towards the level of the 2 C target in Asia, Environ. Pollut., 261, 113650, https://doi.org/10.1016/j.envpol.2019.113650, 2020.

He, Q., Qin, K., Cohen, J. B., Li, D., and Kim, J.: Quantifying Uncertainty in ML-Derived Atmosphere Remote Sensing: Hourly Surface NO2 Estimation With GEMS, Geophys. Res. Lett., 51, e2024GL110468, https://doi.org/10.1029/2024GL110468, 2024.

Hersbach, H., Bell, B., Berrisford, P., Hirahara, S., Horányi, A., Muñoz-Sabater, J., Nicolas, J., Peubey, C., Radu, R., Schepers, D., Simmons, A., Soci, C., Abdalla, S., Abellan, X., Balsamo, G., Bechtold, P., Biavati, G., Bidlot, J., Bonavita, M., De Chiara, G., Dahlgren, P., Dee, D., Diamantakis, M., Dragani, R., Flemming, J., Forbes, R., Fuentes, M., Geer, A., Haimberger, L., Healy, S., Hogan, R. J., Hólm, E., Janisková, M., Keeley, S., Laloyaux, P., Lopez, P., Lupu, C., Radnoti, G., de Rosnay, P., Rozum, I., Vamborg, F., Villaume, S., and Thépaut, J.-N.: The ERA5 global reanalysis, Q. J. R. Meteorol. Soc., 146, 1999–2049, https://doi.org/10.1002/qj.3803, 2020.

Holloway, T., Levy, H., and Kasibhatla, P.: Global distribution of carbon monoxide, J. Geophys. Res. Atmospheres, 105, 12123–12147, https://doi.org/10.1029/1999JD901173, 2000.

Hu, W., Qin, K., Lu, F., Li, D., Cohen, J. B. %J I. J. of C. S., and Technology: Merging TROPOMI and eddy covariance observations to quantify 5-years of daily CH4 emissions over coal-mine dominated region, Int. J. Coal Sci. Technol., 11, 56, https://doi.org/10.1007/s40789-024-00700-1, 2024.

Inness, A., Aben, I., Ades, M., Borsdorff, T., Flemming, J., Jones, L., Landgraf, J., Langerock, B., Nedelec, P., Parrington, M., and Ribas, R.: Assimilation of S5P/TROPOMI carbon monoxide data with the global CAMS near-real-time system, Atmospheric Chem. Phys., 22, 14355–14376, https://doi.org/10.5194/acp-22-14355-2022, 2022.

Jiang, Z., Jones, D. B., Worden, J., Worden, H. M., Henze, D. K., and Wang, Y. X.: Regional data assimilation of multi-spectral MOPITT observations of CO over North America, Atmospheric Chem. Phys., 15, 6801–6814, https://doi.org/10.5194/acp-15-6801-2015, 2015.

Joshi, A., Pathak, M., Kuttippurath, J., and Patel, V. %J C.: Adoption of cleaner technologies and reduction in fire events in the hotspots lead to global decline in carbon monoxide, Chemosphere, 336, 139259, https://doi.org/10.1016/j.chemosphere.2023.139259, 2023.

Khalil, M. A. K. and Rasmussen, R. A.: The global cycle of carbon monoxide: Trends and mass balance, Chemosphere, 20, 227–242, https://doi.org/10.1016/0045-6535(90)90098-E, 1990.

Khalil, M. A. K. and Rasmussen, R. A. %J N.: Carbon monoxide in the Earth's atmosphere: Indications of a global increase, Nature, 332, 242–245, https://doi.org/10.1038/332242a0, 1988.

Khalil, M. A. K. and Rasmussen, R. %J S.: Carbon monoxide in the earth's atmosphere: increasing trend, Science, 224, 54–56, https://doi.org/10.1126/science.224.4644.54, 1984.

Kopacz, M., Jacob, D. J., Henze, D. K., Heald, C. L., Streets, D. G., and Zhang, Q.: Comparison of adjoint and analytical Bayesian inversion methods for constraining Asian sources of carbon monoxide using satellite (MOPITT) measurements of CO columns, J. Geophys. Res. Atmospheres, 114, https://doi.org/10.1029/2007JD009264, 2009.

Kopacz, M., Jacob, D. J., Fisher, J. A., Logan, J. A., Zhang, L., Megretskaia, I. A., Yantosca, R. M., Singh, K., Henze, D. K., and Burrows, J. P.: Global estimates of CO sources with high resolution by adjoint inversion of multiple satellite datasets (MOPITT, AIRS, SCIAMACHY, TES), Atmospheric Chem. Phys., 10, 855–876, https://doi.org/10.5194/acp-10-855-2010, 2010.

https://doi.org/10.5194/egusphere-2025-5890
Preprint. Discussion started: 6 January 2026

Koppmann, R., von Czapiewski, K., and Reid, J. S.: A review of biomass burning emissions, part I: gaseous emissions of carbon monoxide, methane, volatile organic compounds, and nitrogen containing compounds, Atmos Chem Phys Discuss, 2005, 10455–10516, https://doi.org/10.5194/acpd-5-10455-2005, 2005.

Lama, S., Houweling, S., Boersma, K. F., Eskes, H., Aben, I., Denier van der Gon, H. A. C., Krol, M. C., Dolman, H., Borsdorff, T., and Lorente, A.: Quantifying burning efficiency in megacities using the NO2/CO ratio from the Tropospheric Monitoring Instrument (TROPOMI), Atmospheric Chem. Phys., 20, 10295–10310, https://doi.org/10.5194/acp-20-10295-2020, 2020.

Landgraf, J., aan de Brugh, J., Scheepmaker, R., Borsdorff, T., Hu, H., Houweling, S., Butz, A., Aben, I., and Hasekamp, O.: Carbon monoxide total column retrievals from TROPOMI shortwave infrared measurements, Atmospheric Meas. Tech., 9, 4955–4975, https://doi.org/10.5194/amt-9-4955-2016, 2016.

Landgraf, J., Borsdorff, T., Houweling, S., and Hasekamp, O. P.: Algorithm Theoretical Baseline Document for Sentinel-5 Precursor: Carbon Monoxide Total Column Retrieval, 2024.

Landgraf, J., Borsdorff, T., Houweling, S., and Hasekamp, O. P.: Algorithm Theoretical Baseline Document for Sentinel-5 Precursor: Carbon Monoxide Total Column Retrieval, n.d.

Lelieveld, J., Gromov, S., Pozzer, A., and Taraborrelli, D.: Global tropospheric hydroxyl distribution, budget and reactivity, Atmospheric Chem. Phys., 16, 12477–12493, https://doi.org/10.5194/acp-16-12477-2016, 2016.

Li, X., Cohen, J. B., Qin, K., Geng, H., Wu, X., Wu, L., Yang, C., Zhang, R., and Zhang, L.: Remotely sensed and surface measurement- derived mass-conserving inversion of daily NOx emissions and inferred combustion technologies in energy-rich northern China, Atmospheric Chem. Phys., 23, 8001–8019, https://doi.org/10.5194/acp-23-8001-2023, 2023.

Li, X., Cohen, J. B., Tiwari, P., Wu, L., Wang, S., He, Q., Yang, H., and Qin, K.: Space-based inversion reveals underestimated carbon monoxide emissions over Shanxi, Commun. Earth Environ., 6, 1–14, https://doi.org/10.1038/s43247-025-02301-5, 2025.

Liang, L., Wang, Z., and Li, J. %J J. of cleaner production: The effect of urbanization on environmental pollution in rapidly developing urban agglomerations, J. Clean. Prod., 237, 117649, https://doi.org/10.1016/j.jclepro.2019.117649, 2019.

Lin, C., Cohen, J. B., Wang, S., Lan, R., and Deng, W.: A new perspective on the spatial, temporal, and vertical distribution of biomass burning: quantifying a significant increase in CO emissions, Environ. Res. Lett., 15, https://doi.org/10.1088/1748-9326/abaa7a, 2020.

Liu, Q., Gao, Y., Huang, W., Ling, Z., Wang, Z., and Wang, X.: Carbonyl compounds in the atmosphere: A review of abundance, source and their contributions to O3 and SOA formation, Atmospheric Res., 274, 106184, https://doi.org/10.1016/j.atmosres.2022.106184, 2022.

Liu, Z., Cohen, J. B., Wang, S., Wang, X., Tiwari, P., and Qin, K. %J npj C.: Remotely sensed BC columns over rapidly changing Western China show significant decreases in mass and inconsistent changes in number, size, and mixing properties due to policy actions, Npj Clim Atmos Sci, 7, 124, https://doi.org/10.1038/s41612-024-00663-9, 2024.

Liu, Z., Cohen, J. B., Tiwari, P., Guan, L., Wang, S., and Qin, K.: A Global Black Carbon Dataset of Column Concentration and Microphysical Information Derived from MISR Multi-band Observations and Mie Scattering Simulations, Earth Syst Sci Data Discuss, 2025, 1–39, https://doi.org/10.5194/essd-2025-593, 2025.

Lorente, A., Borsdorff, T., Butz, A., Hasekamp, O., aan de Brugh, J., Schneider, A., Wu, L., Hase, F., Kivi, R., Wunch, D., Pollard, D. F., Shiomi, K., Deutscher, N. M., Velazco, V. A., Roehl, C. M., Wennberg, P. O., Warneke, T., and Landgraf, J.: Methane retrieved from TROPOMI: improvement of the data product and validation of the first 2 years of measurements, Atmospheric Meas. Tech., 14, 665–684, https://doi.org/10.5194/amt-14-665-2021, 2021.

Lu, L., Cohen, J. B., Qin, K., Tiwari, P., Hu, W., Gao, H., and Zheng, B.: Observational Uncertainty Causes Over Half of Top-Down Nox Emissions Over Northern China to Be Either Biased or Unreliable, https://doi.org/10.2139/ssrn.4984749, 12 October 2024.

Lui, K. H., Ho, S. S. H., Louie, P. K. K., Chan, C. S., Lee, S. C., Hu, D., Chan, P. W., Lee, J. C. W., and Ho, K. F.: Seasonal behavior of carbonyls and source characterization of formaldehyde (HCHO) in ambient air, Atmos. Environ., 152, 51–60, https://doi.org/10.1016/j.atmosenv.2016.12.004, 2017.

Madrazo, J., Clappier, A., Belalcazar, L. C., Cuesta, O., Contreras, H., and Golay, F.: Screening differences between a local inventory and the Emissions Database for Global Atmospheric Research (EDGAR), Sci. Total Environ., 631–632, 934–941, https://doi.org/10.1016/j.scitotenv.2018.03.094, 2018.

https://doi.org/10.5194/egusphere-2025-5890
Preprint. Discussion started: 6 January 2026

Martínez-Alonso, S., Deeter, M., Worden, H., Borsdorff, T., Aben, I., Commane, R., Daube, B., Francis, G., George, M., Landgraf, J., Mao, D., McKain, K., and Wofsy, S.: 1.5 years of TROPOMI CO measurements: comparisons to MOPITT and ATom, Atmospheric Meas. Tech., 13, 4841–4864, https://doi.org/10.5194/amt-13-4841-2020, 2020.

McDuffie, E. E., Smith, S. J., O'Rourke, P., Tibrewal, K., Venkataraman, C., Marais, E. A., Zheng, B., Crippa, M., Brauer, M., and Martin, R. V.: A global anthropogenic emission inventory of atmospheric pollutants from sector- and fuel-specific sources (1970–2017): an application of the Community Emissions Data System (CEDS), Earth Syst. Sci. Data, 12, 3413–3442, https://doi.org/10.5194/essd-12-3413-2020, 2020.

Munsif, R., Zubair, M., Aziz, A., and Zafar, M. N.: Industrial air emission pollution: potential sources and sustainable mitigation, in: Environmental Emissions, IntechOpen, 2021.

Action Plan for Clean and Efficient Utilization of Coal (2015-2020): http://nyj.jcgov.gov.cn/mtqjgxly/zcwj/202310/t20231005_1863200.shtml, last access: 30 January 2025.

Olivier, J. G. J., Bloos, J. P. J., Berdowski, J. J. M., Visschedijk, A. J. H., and Bouwman, A. F.: A 1990 global emission inventory of anthropogenic sources of carbon monoxide on 1° × 1° developed in the framework of EDGAR/GEIA, Chemosphere - Glob. Change Sci., 1, 1–17, https://doi.org/10.1016/S1465-9972(99)00019-7, 1999.

Patra, P. K., Krol, M. C., Montzka, S. A., Arnold, T., Atlas, E. L., Lintner, B. R., Stephens, B. B., Xiang, B., Elkins, J. W., Fraser, P. J., Ghosh, A., Hintsa, E. J., Hurst, D. F., Ishijima, K., Krummel, P. B., Miller, B. R., Miyazaki, K., Moore, F. L., Mühle, J., O'Doherty, S., Prinn, R. G., Steele, L. P., Takigawa, M., Wang, H. J., Weiss, R. F., Wofsy, S. C., and Young, D.: Observational evidence for interhemispheric hydroxyl-radical parity, Nature, 513, 219–223, https://doi.org/10.1038/nature13721, 2014.

Pirajno, F., Seltmann, R., and Yang, Y.: A review of mineral systems and associated tectonic settings of northern Xinjiang, NW China, Geosci. Front., 2, 157–185, https://doi.org/10.1016/j.gsf.2011.03.006, 2011.

Qin, K., Lu, L., Liu, J., He, Q., Shi, J., Deng, W., Wang, S., and Cohen, J. B.: Model-free daily inversion of NOx emissions using TROPOMI (MCMFE-NOx) and its uncertainty: Declining regulated emissions and growth of new sources, Remote Sens. Environ., 295, 113720, https://doi.org/10.1016/j.rse.2023.113720, 2023.

Rao, K. S.: Uncertainty Analysis in Atmospheric Dispersion Modeling, Pure Appl. Geophys., 162, 1893–1917, https://doi.org/10.1007/s00024-005-2697-4, 2005.

Reilly, J. M., Edmonds, J. A., Gardner, R. H., and Brenkert, A. L.: Uncertainty Analysis of the IEA/ORAU C02 Emissions Model, Energy J., 8, 1–30, https://doi.org/10.5547/ISSN0195-6574-EJ-Vol8-No3-1, 1987.

Röckmann, T., Jöckel, P., Gros, V., Bräunlich, M., Possnert, G., and Brenninkmeijer, C. A. M.: Using 14 C, 13 C, 18 O and 17 O isotopic variations to provide insights into the high northern latitude surface CO inventory, Atmospheric Chem. Phys., 2, 147–159, https://doi.org/10.5194/acp-2-147-2002, 2002.

Rupakheti, D., Yin, X., Rupakheti, M., Zhang, Q., Li, P., Rai, M., and Kang, S.: Spatio-temporal characteristics of air pollutants over Xinjiang, northwestern China, Environ. Pollut., 268, 115907, https://doi.org/10.1016/j.envpol.2020.115907, 2021.

Savenets, M., Dvoretska, I., Nadtochii, L., and Zhemera, N.: Comparison of TROPOMI NO, CO, HCHO, and SO data against ground-level measurements in close proximity to large anthropogenic emission sources in the example of Ukraine, Meteorol. Appl., 29, e2108, https://doi.org/10.1002/met.2108, 2022.

Schneising, O., Buchwitz, M., Reuter, M., Bovensmann, H., Burrows, J. P., Borsdorff, T., Deutscher, N. M., Feist, D. G., Griffith, D. W. T., Hase, F., Hermans, C., Iraci, L. T., Kivi, R., Landgraf, J., Morino, I., Notholt, J., Petri, C., Pollard, D. F., Roche, S., Shiomi, K., Strong, K., Sussmann, R., Velazco, V. A., Warneke, T., and Wunch, D.: A scientific algorithm to simultaneously retrieve carbon monoxide and methane from TROPOMI onboard Sentinel-5 Precursor, Atmospheric Meas. Tech., 12, 6771–6802, https://doi.org/10.5194/amt-12-6771-2019, 2019.

Shepherd, R., King, M., Ward, A., Stuckey, E., Welbourn, R., Brough, N., Milsom, A., Pfrang, C., and Arnold, T.: The lifetimes and potential change in planetary albedo owing to the oxidation of organic films extracted from atmospheric aerosol by hydroyxl (OH) radical oxidation at the air-water interface of aerosol particles, EGUsphere, 2024, 1–37, 2024.

Spivakovsky, C. M., Logan, J. A., Montzka, S. A., Balkanski, Y. J., Foreman-Fowler, M., Jones, D. B. A., Horowitz, L. W., Fusco, A. C., Brenninkmeijer, C. A. M., Prather, M. J., Wofsy, S. C., and McElroy, M. B.: Three-dimensional climatological distribution of tropospheric OH: Update and evaluation, J. Geophys. Res. Atmospheres, 105, 8931–8980, https://doi.org/10.1029/1999jd901006, 2000.

Circular of the State Council on the Issuance of the Action Plan for Continuous Improvement of Air Quality: https://www.gov.cn/zhengce/zhengceku/202312/content_6919001.htm.

https://doi.org/10.5194/egusphere-2025-5890
Preprint. Discussion started: 6 January 2026

Stavrakou, T., Müller, J.-F., Bauwens, M., Doumbia, T., Elguindi, N., Darras, S., Granier, C., Smedt, I. D., Lerot, C., and Van Roozendael, M.: Atmospheric impacts of COVID-19 on NOx and VOC levels over China based on TROPOMI and IASI satellite data and modeling, Atmosphere, 12, 946, https://doi.org/10.3390/atmos12080946, 2021.

Sun, J., He, Y., Ning, Y., Xue, Z., Wang, H., Zhang, Y., Ma, J., Chen, X., and Chai, F.: Pollution characteristics and sources of carbonyl compounds in a typical city of Fenwei Plain, Linfen, in summer, Environ. Pollut., 320, 120913, https://doi.org/10.1016/j.envpol.2022.120913, 2023.

Szopa, S., Naik, V., Adhikary, B., Artaxo, P., Berntsen, T., Collins, W. D., Fuzzi, S., Gallardo, L., Kiendler-Scharr, A., and Klimont, Z.: Short-Lived Climate Forcers (Chapter 6), in: Climate Change 2021 – The Physical Science Basis, Cambridge University Press, 2021.

Tian, Y., Liu, C., Sun, Y., Borsdorff, T., Landgraf, J., Lu, X., Palm, M., and Notholt, J.: Satellite Observations Reveal a Large CO Emission Discrepancy From Industrial Point Sources Over China, Geophys. Res. Lett., 49, e2021GL097312, https://doi.org/10.1029/2021GL097312, 2022.

Veefkind, J. P., Aben, I., McMullan, K., Förster, H., De Vries, J., Otter, G., Claas, J., Eskes, H. J., De Haan, J. F., Kleipool, Q., Van Weele, M., Hasekamp, O., Hoogeveen, R., Landgraf, J., Snel, R., Tol, P., Ingmann, P., Voors, R., Kruizinga, B., Vink, R., Visser, H., and Levelt, P. F.: TROPOMI on the ESA Sentinel-5 Precursor: A GMES mission for global observations of the atmospheric composition for climate, air quality and ozone layer applications, Remote Sens. Environ., 120, 70–83, https://doi.org/10.1016/j.rse.2011.09.027, 2012.

Wang, C., Wang, T., Wang, P., and Wang, W.: Assessment of the Performance of TROPOMI NO2 and SO2 Data Products in the North China Plain: Comparison, Correction and Application, Remote Sens., 14, 214, https://doi.org/10.3390/rs14010214, 2022.

Wang, S. and Cohen, J. B.: Reconstructing Decade-long NO2 and CO Emissions at Global Scale Combining a New Constrained Top-down Approach, Measurements, and Models, AGU Fall Meeting Abstracts, GC21K-1067, 2023.

Wang, S., Cohen, J. B., Deng, W., Qin, K., and Guo, J.: Using a New Top-Down Constrained Emissions Inventory to Attribute the Previously Unknown Source of Extreme Aerosol Loadings Observed Annually in the Monsoon Asia Free Troposphere, Earths Future, 9, e2021EF002167, https://doi.org/10.1029/2021EF002167, 2021.

Wang, S., Cohen, J., Guan, L., Lu, L., Tiwari, P., and Qin, K.: Observationally Constrained Emissions Variability Contributes Significantly to Global NOx, CO, and CO2 Emissions, https://doi.org/10.21203/rs.3.rs-4948370/v1, 24 September 2024.

Wei, C., Wang, M., Fu, Q., Dai, C., Huang, R., and Bao, Q.: Temporal characteristics of greenhouse gases (CO2 and CH4) in the megacity Shanghai, China: Association with air pollutants and meteorological conditions, Atmospheric Res., 235, 104759, https://doi.org/10.1016/j.atmosres.2019.104759, 2020.

Worden, H. M., Deeter, M. N., Frankenberg, C., George, M., Nichitiu, F., Worden, J., Aben, I., Bowman, K. W., Clerbaux, C., and Coheur, P.-F.: Decadal record of satellite carbon monoxide observations, Atmospheric Chem. Phys., 13, 837–850, https://doi.org/10.5194/acp-13-837-2013, 2013.

World Health Organization: WHO global air quality guidelines: particulate matter (PM2. 5 and PM10), ozone, nitrogen dioxide, sulfur dioxide and carbon monoxide, World Health Organization, 2021.

Yang, Y., Wang, Y., Huang, W., Yao, D., Zhao, S., Wang, Y., Ji, D., Zhang, R., and Wang, Y.: Parameterized atmospheric oxidation capacity and speciated OH reactivity over a suburban site in the North China Plain: A comparative study between summer and winter, Sci. Total Environ., 773, 145264, https://doi.org/10.1016/j.scitotenv.2021.145264, 2021.

Yin, Y., Chevallier, F., Ciais, P., Broquet, G., Fortems-Cheiney, A., Pison, I., and Saunois, M.: Decadal trends in global CO emissions as seen by MOPITT, Atmospheric Chem. Phys., 15, 13433–13451, https://doi.org/10.5194/acp-15-13433-2015, 2015.

Zeng, Q. and Shen, L.: Experimental study on the oxidation kinetics of coal in typical coal mining areas of the Southern Junggar coalfield, Xinjiang, China, Int. J. Coal Sci. Technol., 9, 78, https://doi.org/10.1007/s40789-022-00542-9, 2022.

Zhang, F., Zhou, L. X., Novelli, P. C., Worthy, D. E. J., Zellweger, C., Klausen, J., Ernst, M., Steinbacher, M., Cai, Y. X., Xu, L., Fang, S. X., and Yao, B.: Evaluation of in situ measurements of atmospheric carbon monoxide at Mount Waliguan, China, Atmospheric Chem. Phys., 11, 5195–5206, https://doi.org/10.5194/acp-11-5195-2011, 2011.

Zhang, L., Jacob, D. J., Bowman, K. W., Logan, J. A., Turquety, S., Hudman, R. C., Li, Q., Beer, R., Worden, H. M., Worden, J. R., Rinsland, C. P., Kulawik, S. S., Lampel, M. C., Shephard, M. W., Fisher, B. M., Eldering, A., and Avery, M. A.: Ozone-CO correlations determined by the TES satellite instrument in continental outflow regions, Geophys. Res. Lett., 33, https://doi.org/10.1029/2006GL026399, 2006.

https://doi.org/10.5194/egusphere-2025-5890
Preprint. Discussion started: 6 January 2026

Zhao, Y., Nielsen, C. P., McElroy, M. B., Zhang, L., and Zhang, J.: CO emissions in China: uncertainties and implications of improved energy efficiency and emission control, Atmos. Environ., 49, 103–113, 2012.

Zhao, Z., He, Q., Lu, Z., Zhao, Q., and Wang, J.: Analysis of Atmospheric CO2 and CO at Akedala Atmospheric Background Observation Station, a Regional Station in Northwestern China, Int. J. Environ. Res. Public. Health, 19, 6948, https://doi.org/10.3390/ijerph19116948, 2022.

Zheng, B., Chevallier, F., Ciais, P., Yin, Y., Deeter, M. N., Worden, H. M., Wang, Y., Zhang, Q., and He, K.: Rapid decline in carbon monoxide emissions and export from East Asia between years 2005 and 2016, Environ. Res. Lett., 13, 044007, https://doi.org/10.1088/1748-9326/aab2b3, 2018a.

Zheng, B., Tong, D., Li, M., Liu, F., Hong, C., Geng, G., Li, H., Li, X., Peng, L., and Qi, J.: Trends in China's anthropogenic emissions since 2010 as the consequence of clean air actions, Atmospheric Chem. Phys., 18, 14095–14111, https://doi.org/10.5194/acp-18-14095-2018, 2018b.

Zheng, B., Zhang, Q., Geng, G., Chen, C., Shi, Q., Cui, M., Lei, Y., and He, K.: Changes in China's anthropogenic emissions and air quality during the COVID-19 pandemic in 2020, Earth Syst. Sci. Data, 13, 2895–2907, https://doi.org/10.5194/essd-13-2895-2021, 2021.

Zheng, B., Cohen, J. B., Lu, L., Hu, W., Tiwari, P., Wong, M. S., and Qin, K.: Methane Emissions Computed Including Explicit Observational Uncertainty Reveal Bias, Large Number of Unreliable Pixels, https://doi.org/10.22541/essoar.172118448.85241948/v1, 2024.